Environmentally-induced Rabi oscillations and decoherence in superconducting phase qubits

Kaushik Mitra, C. J. Lobb, and C. A. R. Sá de Melo
Department of Physics and Joint Quantum Institute, University of Maryland, College Park, Maryland 20742, USA
(Received 26 March 2009; published 30 April 2009)

We study decoherence effects in qubits coupled to environments that exhibit resonant frequencies in their spectral function. We model the coupling of the qubit to its environment via the Caldeira-Leggett formulation of quantum dissipation/coherence, and study the simplest example of decoherence effects in circuits with resonances such as a dc superconducting quantum interference device (SQUID) phase qubit in the presence of an isolation circuit. Using the dc SQUID phase qubit as an example, we obtain two quite general results. First, when the frequency of the qubit is at least two times larger than the resonance frequency of the environmental spectral density (the isolation circuit in the case of a dc SQUID phase qubit), we find that the decoherence time of the qubit is a few orders of magnitude larger than that of the typical Ohmic regime, where the frequency of the qubit is much smaller than the resonance frequency of the spectral density. Second, we show that, when the qubit frequency is nearly the same as the resonant frequency of the environmental spectral density, an oscillatory non-Markovian decay emerges, as the qubit and its environment self-generate Rabi oscillations of characteristic time scales shorter than the decoherence time.

DOI: 10.1103/PhysRevB.79.132507 PACS number(s): 74.50.+r, 03.67.Lx, 85.25.Dq

The possibility of using quantum mechanics to manipulate information efficiently has lead, through advances in technology, to the plausibility of building a quantum computer using two-level systems, also called quantum bits or qubits. Several schemes have been proposed as attempts to manipulate qubits in atomic, molecular, and optical physics (AMO), and condensed-matter physics (CMP).

In AMO, the most promising schemes are trapped ion systems,[1] and ultracold atoms in optical lattices.[2] On the CMP side, the pursuit of solid-state qubits has been quite promising in spin systems[3,4] and superconducting devices.[5–7] While the manipulation of qubits in AMO has relied on the existence of qubits in a lattice of ions or ultracold atoms and the use of lasers, the manipulation of qubits in CMP has relied on the NMR techniques (spin qubits) and the Josephson effect (superconducting qubits). Integrating qubits into a full quantum computer requires a deeper understanding of decoherence effects in a single qubit and how different qubits couple.

In AMO systems Rabi oscillations in single qubits have been observed over time scales of milliseconds since each qubit can be made quite isolated from its environment;[1] however it has been very difficult to implement multiqubit states as the coupling between different qubits is not yet fully controllable. On the other hand, in superconducting qubits Rabi oscillations have been observed[5,8] over shorter time scales (500 ns) since these qubits are coupled to many environmental degrees of freedom, and require very careful circuit design. For superconducting qubits, it has been shown experimentally[8] that sources of decoherence from two-level states within the insulating barrier of a Josephson junction can be significantly reduced by using better dielectrics and fabricating junctions of small area ($\lesssim 10\ \mu m^2$).

In this Brief Report, we analyze decoherence effects of generic qubits coupled to environments that exhibit a resonance in their spectral density within the Caldeira-Leggett formulation of quantum dissipation. Because of space limitations, we discuss only the specific example of a single superconducting phase qubit coupled to isolation circuits with a resonance. However, we can show[9] that there are additional examples of qubits coupled to environments exhibiting resonances such as the persistent current (flux) qubits[10,11] coupled to a read-out superconducting quantum interference device (SQUID) or charge qubits[12] coupled to a dissipative cavity. The general idea, presented in this Brief Report, is applicable to all such superconducting qubits which are coupled to environments exhibiting resonances.

The example circuit used to describe intrinsic decoherence and self-induced Rabi oscillations in qubits is shown in Fig. 1, which corresponds to an asymmetric dc SQUID.[13,14] The circuit elements inside the dashed box form an isolation network which serves two purposes: (a) it prevents current noise from reaching the qubit junction and (b) it is used as a measurement tool.

The classical equation of motion for such a circuit is

$$C_0\ddot{\gamma}+\frac{2\pi}{\Phi_0}I_{c0}\sin\gamma-\frac{2\pi}{\Phi_0}I+\int_0^t dt' Y(t-t')\dot{\gamma}(t')=0, \quad (1)$$

where C_0 is the capacitance, I_{c0} is the critical current, and γ is the phase difference across the Josephson junction J in Fig. 1 while I is the bias current, and $\Phi_0=h/2e$ is the flux quantum. The last term of Eq. (1) can be written as $i\omega Y(\omega)\gamma(\omega)$ in Fourier space. The admittance function $Y(\omega)$ can be modeled as two additive terms $Y(\omega)=Y_{\rm iso}(\omega)+Y_{\rm int}(\omega)$. The first contribution $Y_{\rm iso}(\omega)$ is the admittance that results when a transmission line of characteristic impedance

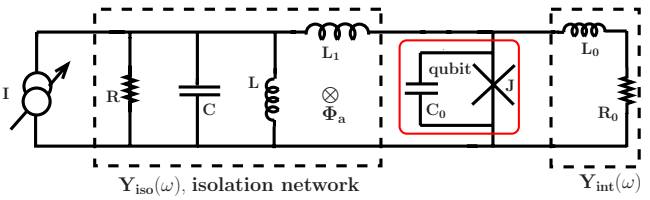

FIG. 1. (Color online) Schematic drawing of the phase qubit with an *RLC* isolation circuit.

R is attached to the isolation junction (here represented by a capacitance C and a Josephson inductance L) and an isolation inductance L_1. Thus, $Y_{\rm iso}(\omega)=Z_{\rm iso}^{-1}(\omega)$ where $Z_{\rm iso}(\omega)=(i\omega L_1)+[R^{-1}+i\omega C+(i\omega L)^{-1}]^{-1}$ is the impedance of the isolation network shown in Fig. 1. The replacement of the isolation junction by an LC circuit is justified because under standard operating conditions the external flux Φ_a varies to cancel the current flowing through the isolation junction making it zero biased.[13] Thus, the isolation junction behaves as a harmonic oscillator with inductance L which is chosen to be much smaller than L_1. The second contribution $Y_{\rm int}(\omega)$ is an internal admittance representing the local environment of the qubit junction, such as defects in the oxide barrier, quasiparticle tunneling, or the substrate, and can be modeled by $Y_{\rm int}(\omega)=(R_0+i\omega L_0)^{-1}$, where R_0 is the resistance and L_0 is the inductance of the qubit as shown in Fig. 1.

Next, we use the Caldeira-Leggett formalism to describe the coupling of the phase qubit to the isolation network, via the spin-boson Hamiltonian[15]

$$\tilde{H}=\frac{\hbar\omega_{01}}{2}\sigma_z+\sum_k \hbar\omega_k b_k^\dagger b_k+H_{\rm SB}, \tag{2}$$

written in terms of Pauli matrices σ_i (with $i=x,y,z$), and boson operators b_k and $b_k^\dagger$. The first term in Eq. (2) represents a two-level approximation for the phase qubit (system) described by states $|0\rangle$ and $|1\rangle$ with energy difference $\hbar\omega_{01}=\sqrt{8E_cE_J}(1-I^2/I_{c0}^2)^{1/4}$, where $E_c=(2e)^2/2C$ is the capacitive energy, and $E_J=(\Phi_0/2\pi)I_{c0}$ is the Josephson energy. The second term corresponds to the isolation network represented by a bath of bosons, where b_k and $b_k^\dagger$ are the annihilation and creation operators of the kth bath mode with frequency ω_k. The third term is the system-bath (SB) Hamiltonian

$$H_{\rm SB}=\frac{1}{2}\sigma_x\hbar\langle 1|\gamma|0\rangle\sum_k \lambda_k(b_k^\dagger+b_k), \tag{3}$$

corresponding to the coupling between the isolation network and the phase qubit which appears as $\int_0^t dt' Y(t-t')\dot{\gamma}(t')$ in the classical equation of motion [Eq. (1)].

The spectral density of the bath modes $J(\omega)=\hbar\Sigma_k\lambda_k^2\delta(\omega-\omega_k)$ has dimensions of energy and can be written as $J(\omega)=\omega\,\mathrm{Re}\,Y(\omega)(\Phi_0/2\pi)^2$, which leads to the compact form $J(\omega)=J_{\rm iso}(\omega)+J_{\rm int}(\omega)$. The spectral density of the isolation network is

$$J_{\rm iso}(\omega)=\left(\frac{\Phi_0}{2\pi}\right)^2\frac{\alpha\omega}{(1-\omega^2/\Omega^2)^2+4\omega^2\Gamma^2/\Omega^4}, \tag{4}$$

where $\alpha=L^2/[(L+L_1)^2R]\approx(L/L_1)^2/R$ is the leading-order term in the low-frequency Ohmic regime, $\Omega=\sqrt{(L+L_1)/(LL_1C)}\approx 1/\sqrt{LC}$ is essentially the resonance frequency, and $\Gamma=1/(2CR)$ plays the role of resonance width. Here, we used $L_1\gg L$ corresponding to the relevant experimental regime. Notice that $J_{\rm iso}(\omega)$ has Ohmic behavior at low frequencies $\lim_{\omega\to 0}J_{\rm iso}(\omega)/\omega=(\Phi_0/2\pi)^2(L/L_1)^2/R$ but has a peak at frequency Ω with broadening controlled by Γ. In addition, notice that the dimensionless parameter $\Gamma/\Omega^2=LL_1/[2R(L_1+L)]\approx R/L$ is independent of C. Therefore, when there is no capacitor ($C\to 0$), the resonance disappears and

$$J_{\rm iso}(\omega)=\left(\frac{\Phi_0}{2\pi}\right)^2\frac{\alpha\omega}{1+4\omega^2\Gamma^2/\Omega^4} \tag{5}$$

reduces to a Drude term with characteristic frequency $\Omega^2/2\Gamma\approx R/L$. The internal spectral density of the qubit is

$$J_{\rm int}(\omega)=\left(\frac{\Phi_0}{2\pi}\right)^2\frac{(\omega/R_0)}{1+\omega^2L_0^2/R_0^2}, \tag{6}$$

which is a Drude term with characteristic frequency R_0/L_0. Notice that $J_{\rm int}(\omega)$ also has Ohmic behavior at low frequencies $\lim_{\omega\to 0}J_{\rm int}(\omega)/\omega=(\Phi_0/2\pi)^2/R_0$. In order to obtain the relaxation T_1 and decoherence T_2 times, we write the Bloch-Redfield equations,[16]

$$\dot{\rho}_{nm}=-i\omega_{nm}\rho_{nm}+\sum_{kl}R_{nmkl}\rho_{kl}, \tag{7}$$

for the density matrix ρ_{nm} of the spin-boson Hamiltonian in Eqs. (2) and (3) derived in the Born-Markov limit. Here all indices take the values 0 and 1 corresponding to the ground and excited states of the qubit, respectively, while $\omega_{nm}=(E_n-E_m)/\hbar$ is the frequency difference between states n and m. The Redfield rate tensor is

$$R_{nmkl}=-\Gamma^{(1)}_{lmnk}-\Gamma^{(2)}_{lmnk}+\delta_{nk}\Gamma^{(1)}_{lrrm}+\delta_{lm}\Gamma^{(2)}_{nrrk}, \tag{8}$$

where repeated indices indicate summation, and

$$\Gamma^{(1)}_{lmnk}=\hbar^{-2}\int_0^\infty dt e^{-i\omega_{nk}t}\langle H_{{\rm SB},lm}(t)H_{{\rm SB},nk}(0)\rangle, \tag{9}$$

$$\Gamma^{(2)}_{lmnk}=\hbar^{-2}\int_0^\infty dt e^{-i\omega_{lm}t}\langle H_{{\rm SB},lm}(0)H_{{\rm SB},nk}(t)\rangle. \tag{10}$$

Under these conditions, the relaxation rate $1/T_1=-\Sigma_n R_{nnnn}$ becomes

$$\frac{1}{T_1}=\frac{1}{M\omega_{01}}J(\omega_{01})\coth\left(\frac{\hbar\omega_{01}}{k_BT}\right), \tag{11}$$

where $M\equiv(\Phi_0/2\pi)^2C_0$ has dimensions of mass $\times$ area (or energy $\times$ time squared) and is referred to as the *mass* of the phase qubit with capacitance C_0, while ω_{01} is the qubit frequency.

In Fig. 2, T_1 is plotted versus qubit frequency ω_{01} for spectral densities describing an RLC [Eq. (4)] or Drude [Eq. (5)] isolation network at fixed temperatures $T=0$ (main figure) and $T=50$ mK (inset), for $J_{\rm int}(\omega)=0$ corresponding to $R_0\to\infty$. In the limit of low temperatures ($k_BT/\hbar\omega_{01}\ll 1$), the relaxation time becomes $T_1(\omega_{01})=M\omega_{01}/J(\omega_{01})$. From Fig. 2 (main plot) several important points can be extracted. First, in the low-frequency regime ($\omega_{01}\ll\Omega$), the RL (Drude) and RLC environments produce essentially the same relaxation time $T_{1,RLC}(0)=T_{1,RL}(0)=T_{1,0}\approx(L_1/L)^2RC_0$, because both systems are Ohmic. Second, near resonance ($\omega_{01}\approx\Omega$), $T_{1,RLC}$ is substantially reduced because the qubit is resonantly coupled to its environment producing a distinct non-Ohmic behavior. Third, for ($\omega_{01}>\Omega$), T_1 grows very rapidly

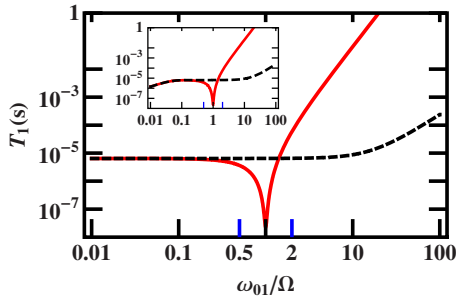

FIG. 2. (Color online) T_1 (in seconds) as a function of qubit frequency ω_{01}. The solid (red) curves describes an *RLC* isolation network with parameters $R=50\ \Omega$, $L_1=3.9$ nH, $L=2.25$ pH, and $C=2.22$ pF, and qubit parameters $C_0=4.44$ pF, $R_0=\infty$, and $L_0=0$. The dashed curves correspond to an *RL* isolation network with the same parameters except that $C=0$. Main figure ($T=0$) and the inset ($T=50$ mK) with $\Omega=141\times10^9$ rad/s.

in the *RLC* case. Notice that for $\omega_{01}>\sqrt{2}\Omega$, the *RLC* relaxation time $T_{1,RLC}$ is always larger than $T_{1,RL}$. Furthermore, in the limit of $\omega_{01}\gg\max\{\Omega,2\Gamma\}$, $T_{1,RLC}$ grows with the fourth power of ω_{01} behaving as $T_{1,RLC}\approx T_{1,0}\omega_{01}^4/\Omega^4$, while for $\omega_{01}\gg\Omega^2/2\Gamma$, $T_{1,RL}$ grows only with second power of ω_{01} behaving as $T_{1,RL}\approx 4T_{1,0}\Gamma^2\omega_{01}^2/\Omega^4$. Thus, $T_{1,RLC}$ is always much larger than $T_{1,RL}$ for sufficiently large ω_{01}. For parameters in the experimental range (Fig. 2), $T_{1,RLC}$ is two orders of magnitude larger than $T_{1,RL}$, indicating a clear advantage of the *RLC* environment shown in Fig. 1 over the standard Ohmic *RL* environment. Thermal effects are shown in the inset of Fig. 2, where $T=50$ mK is a characteristic experimental temperature.[17] Typical values of T_1 at low frequencies vary from 10^{-5} s at $T=0$ to 10^{-6} s at $T=50$ mK while the high-frequency values remain essentially unchanged as thermal effects are not important for $\hbar\omega_{01}\gg k_BT$.

In the preceding analysis we neglected the effect of the local environment by setting $Y_{\rm int}(\omega)=0$. As a result, the low-frequency value of T_1 is substantially larger than obtained in experiment.[13,17] By modeling the local environment with $R_0=5000\ \Omega$ and $L_0=0$, we obtain the T_1 versus ω_{01} plot shown in Fig. 3. Notice that this value of R_0 brings T_1 to values close to 20 ns at $T=0$. The message to extract from

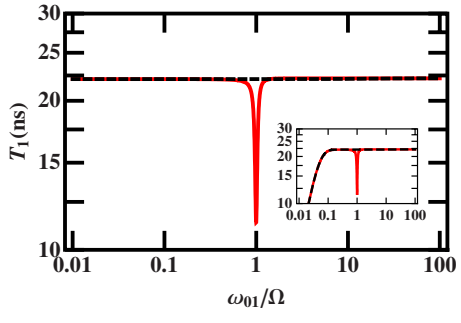

FIG. 3. (Color online) T_1 (in nanoseconds) as a function of qubit frequency ω_{01}. The solid (red) curves describes an *RLC* isolation network for same parameters of Fig. 2 except that $R_0=5000\ \Omega$. The dashed curves correspond to an *RL* isolation network with the same parameters of the *RLC* network, except that $C=0$. Main figure ($T=0$) and the inset ($T=50$ mK) with $\Omega=141\times10^9$ rad/s.

Figs. 2 and 3 is that increasing R_0 as much as possible and increasing the qubit frequency ω_{01} from 0.1 to 2 Ω at fixed low temperature can produce a large increase in T_1.

The Bloch-Redfield equations described in Eq. (7) capture the long-time behavior of the density matrix but cannot describe the short-time behavior of the system in particular near a resonance where $\omega_{01}\approx\Omega$, where the *RLC* spectral density is very large. In this case, only the environmental modes with $\omega_k=\Omega$ couple strongly to the two-level system, like a two-level atom interacting with an electromagnetic field cavity mode that has a finite lifetime. This is best seen by restricting the Hamiltonian described in Eqs. (2) and (3) only to boson modes with $\omega_k\approx\Omega\approx\omega_{01}$, and rewriting the spectral density as

$$J_{\rm iso}(\omega)=\left(\frac{\Phi_0}{2\pi}\right)^2\frac{\alpha\Omega^3}{4{\rm i}\Gamma}\sum_{\sigma=\pm1}\frac{\sigma\omega}{\omega^2-(\sigma\tilde{\Omega}+{\rm i}\Gamma)^2},\qquad(12)$$

where α has the same definition as in Eq. (4), and $\tilde{\Omega}=\Omega-\Gamma^2/\Omega$. This reveals a resonance at $\omega=\tilde{\Omega}$ with linewidth Γ, such that $J_{\rm int}(\omega=\tilde{\Omega})$ can be neglected for any nonzero value of R_0, and $J(\omega)\approx J_{\rm iso}(\omega)$.

When $\omega_k\approx\Omega\approx\omega_{01}$, the Hamiltonian in Eqs. (2) and (3) can be solved in the rotating wave approximation using the complete basis set of system-bath product states $|\psi_0\rangle=|0\rangle_{\rm S}\otimes|0\rangle_{\rm B}$, $|\psi_1\rangle=|1\rangle_{\rm S}\otimes|0\rangle_{\rm B}$, and $|\psi_k\rangle=|0\rangle_{\rm S}\otimes|k\rangle_{\rm B}$, where $|0\rangle_{\rm S}$ and $|1\rangle_{\rm S}$ are the states of the qubit and $|k\rangle_{\rm B}$ are the states of the bath. Notice that the states $|1\rangle_{\rm S}\otimes|k\rangle_{\rm B}$ are absent in the basis set within the rotating wave approximation and the state of the total system at any time is

$$\phi(t)=c_0\psi_0+c_1(t)\psi_1+\sum_{k\neq0,1}c_k(t)\psi_k,\qquad(13)$$

with probability amplitudes c_0, $c_1(t)$, and $c_k(t)$. The amplitude c_0 is constant while the amplitudes $c_1(t)$ and $c_k(t)$ are time dependent. Assuming that there are no excited bath modes at $t=0$, we impose the initial condition $c_k(0)=0$, and use the normalization $|\phi(t)|^2=1$ to obtain the closed integrodifferential equation

$$\dot{c}_1(t)=-\int_0^t dt_1 f(t-t_1)c_1(t_1),\qquad(14)$$

where the kernel is the correlation function,

$$f(\tau)=\int d\omega J(\omega)\exp[{\rm i}(\omega_{01}-\omega)\tau],$$

directly related to the spectral density $J(\omega)$. In the present case the reduced density matrix is

$$\rho(t)=\begin{pmatrix}|c_1(t)|^2 & c_1(t)c_0^*\\ c_1^*(t)c_0 & |c_0|^2+\sum_k|c_k(t)|^2\end{pmatrix}.\qquad(15)$$

which in combination with the condition that $|c_0|^2+\Sigma_k|c_k(t)|^2=1-|c_1(t)|^2$(Tr $\rho(t)=1$) indicates that the time dynamics of $\rho(t)$ is fully determined by $c_1(t)$.

We can now solve for $c_1(t)$ exactly and obtain the closed form

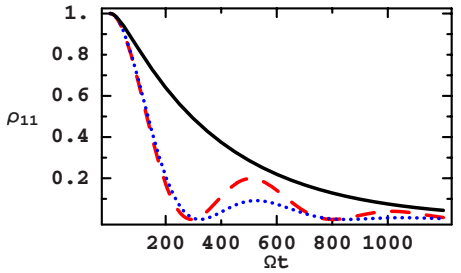

FIG. 4. (Color online) Population of the excited state of the qubit as a function of time $\rho_{11}(t)$, with $\rho_{11}(t=0)=1$ for $R=50\ \Omega$, (solid curve), 350 Ω (dotted curve), and $R=550\ \Omega$ (dashed curve), and $L_1=3.9$ nH, $L=2.25$ pH, $C=2.22$ pF, $C_0=4.44$ pF, $R_0=\infty$, and $L_0=0$.

$$c_1(t) = \mathcal{L}^{-1}\left\{ \frac{(s+\Gamma-i\omega_{01})^2+\Omega^2-\Gamma^2}{s[(s+\Gamma-i\omega_{01})^2+\Omega^2-\Gamma^2]-\kappa\Omega^4\pi i/\Gamma} \right\},$$

where $\mathcal{L}^{-1}\{F(s)\}$ is the inverse Laplace transform of $F(s)$, and $\kappa=(\alpha/M\omega_{01})\times(\Phi_0/2\pi)^2\approx 1/(\omega_{01}T_{1,0})$. The element $\rho_{11}=|c_1(t)|^2$ of the density matrix is plotted in Fig. 4 for three different values of resistance, assuming that the qubit is in its excited state such that $\rho_{11}(0)=1$. We consider the experimentally relevant weak dissipation limit of $\Gamma \ll \omega_{01}\approx\Omega$. Since $\Gamma=1/(2CR)$ the width of the resonance in the spectral density shown in Eq. (12) is smaller for larger values of R. Thus, for large R, the *RLC* environment transfers energy resonantly back and forth to the qubit and induces Rabi oscillations with an effective time dependent decay rate $\gamma(t)=-2\mathcal{R}\{\dot{c}_1(t)/c_1(t)\}$.

These environmentally-induced Rabi oscillations are a clear signature of the non-Markovian behavior produced by the *RLC* environment, and are completely absent in the *RL* environment because the energy from the qubits is quickly dissipated without being temporarily stored. These environmentally-induced Rabi oscillations are generic features of circuits with resonances in the real part of the admittance. The frequency of the Rabi oscillations $\Omega_{\mathrm{Ra}}=\sqrt{\pi\kappa\Omega^3/2\Gamma}$ is independent of the resistance since $\Omega_{\mathrm{Ra}}\approx\Omega\sqrt{\pi L^2C/L_1^2C_0}$, and has the value of $\Omega_{\mathrm{Ra}}=2\pi f_{\mathrm{Ra}}\approx 360\times 10^6$ rad/s for Fig. 4. In fact this effect is similar to the so-called circuit quantum electrodynamics which has been of great experimental interest recently.[18–20]

In conclusion, we analyzed decoherence effects in qubits coupled to environments containing resonances in their spectral function. As an example, we studied a single superconducting phase qubit coupled to isolation circuits with an intrinsic resonance, and emphasized the crucial role played by the design of the isolation circuit on decoherence properties. In particular, for an *RLC* isolation circuit, we found that the decoherence time of the qubit is two orders of magnitude larger than its typical low-frequency Ohmic regime, provided that the frequency of the qubit is about two times larger than the resonance frequency of the isolation circuit. Lastly, we showed that, when the qubit frequency is close to a resonance of the environment (isolation circuit), the nonoscillatory Markovian decay of the excited-state population of the qubit gives in to an oscillatory non-Markovian decay, as the phase qubit and its environment self-generate Rabi oscillations of characteristic time scales shorter than the decoherence time.

We acknowledge support from NSF (Contract No. DMR-0304380) and NSA, through the Laboratory of Physical Sciences.

[1] C. Monroe, D. M. Meekhof, B. E. King, W. M. Itano, and D. J. Wineland, Phys. Rev. Lett. **75**, 4714 (1995).
[2] G. K. Brennen, C. M. Caves, P. S. Jessen, and I. H. Deutsch, Phys. Rev. Lett. **82**, 1060 (1999).
[3] R. Hanson, B. Witkamp, L. M. K. Vandersypen, L. H. Willems van Beveren, J. M. Elzerman, and L. P. Kouwenhoven, Phys. Rev. Lett. **91**, 196802 (2003).
[4] T. Hayashi, T. Fujisawa, H. D. Cheong, Y. H. Jeong, and Y. Hirayama, Phys. Rev. Lett. **91**, 226804 (2003).
[5] D. Vion *et al.*, Science **296**, 886 (2002).
[6] R. C. Ramos *et al.*, IEEE Trans. Appl. Supercond. **11**, 998 (2001).
[7] A. Shnirman, G. Schon, and Z. Hermon, Phys. Rev. Lett. **79**, 2371 (1997).
[8] J. Martinis *et al.*, Phys. Rev. Lett. **95**, 210503 (2005).
[9] K. Mitra, C. J. Lobb, and C. A. R. Sá de Melo, arXiv:0805.2419 (unpublished).
[10] J. E. Mooij *et al.*, Science **285**, 1036 (1999).
[11] C. H. van der Wal *et al.*, Eur. Phys. J B **31**, 111 (2003).
[12] J. Koch, T. M. Yu, J. Gambetta, A. A. Houck, D. I. Schuster, J. Majer, A. Blais, M. H. Devoret, S. M. Girvin, and R. J. Schoelkopf, Phys. Rev. A **76**, 042319 (2007).
[13] J. M. Martinis, S. Nam, J. Aumentado, and C. Urbina, Phys. Rev. Lett. **89**, 117901 (2002).
[14] J. M. Martinis, S. Nam, J. Aumentado, K. M. Lang, and C. Urbina, Phys. Rev. B **67**, 094510 (2003).
[15] A. J. Leggett *et al.*, Rev. Mod. Phys. **59**, 1 (1987).
[16] U. Weiss, *Quantum Dissipative Systems* (World Scientific, Singapore, 1999).
[17] Hanhee Paik *et al.*, Phys. Rev. B **77**, 214510 (2008).
[18] A. Wallraff *et al.*, Nature (London) **431**, 162 (2004).
[19] I. Chiorescu *et al.*, Nature (London) **431**, 159 (2004).
[20] M. A. Sillanpaa *et al.*, Nature (London) **449**, 438 (2007).